UNIVERSIDADE DE SÃO PAULO

INSTITUTO DE FÍSICA
CAIXA POSTAL 20516
01498 - SÃO PAULO - SP
BRASIL

PUBLICAÇÕES

IFUSP/P-924

LUMINESCENCE QUENCHING BY IRON IN BARIUM ALUMINOBORATE GLASSES

Sheila Maria Del Nery, Walter Maigon Pontuschka, Sadao Isotani
Instituto de Física, Universidade de São Paulo

Collin G. Rouse
Instituto de Pesquisas Tecnológicas

Junho/1991

LUMINESCENCE QUENCHING BY IRON IN BARIUM ALUMINOBORATE GLASSES

Sheila Maria Del Nery, Walter Maigon Pontuschka, Sadao Isotani

Instituto de Física, Universidade de São Paulo

C.P. 20516, 01498 São Paulo, SP, Brasil

Collin G. Rouse

Instituto de Pesquisas Tecnológicas

PACS–90: 78.60kn

ABSTRACT

The quenching of luminescence which occurs in barium aluminoborate glass containing iron impurity was investigatted using EPR and TL measurements. The EPR spectra showed Fe^{3+} at substitutional site of boron atoms in double tetrahedral B_2O_7 units. The activation energy of electron untrapping from the BEC was determined from TL measurements using initial rise to be about 0.21 eV. The TL measurements also exhibited an exponential decrease of the TL intensity in function of Fe concentration. The exponential correlation between the TL intensity and the Fe concentration was explained with the support of recent theories about non–radiactive electron–hole recombination mechanism.

I. INTRODUCTION

Irradiated barium aluminoborate glass show red phosphorescence at temperatures above 400°C [1]. At room temperature EPR measurements show that BEC (boron electron centers) are absent, remaining only BOHC (boron oxygen hole centers). This observation was used to propose a model of hole–ion recombination luminescence, and show that BOHC has low mobility at room and at lower temperatures. The ion could be Fe^{2+}, which is found in small amounts in these glasses [2].

Phosphorescence at temperatures below the ambient was also observed in barium aluminoborate glass [3,4]. In this case the phosphorescence was attributed to the electron–hole recombination. Electrons released from BEC recombine with holes at BOHC, with the excess of energy giving rise low temperature phosphorescence.

The killing effect of luminescence due to impurities in crystals was subject of extensive studies. The first developed model was the competitive capture of free electrons at two different centers emitting at different wavelengths [5,6] with a linear correlation between intensity of excitation and luminescence. However, experimentally this correlation is not always linear [7–10], which was explained with a model of excitation and recombination [11] with different cross section of capture of carriers [12]. From 1964, the luminescence studies found a new focus, because the non–radiative recombination was suggested as the origin of the enlargement of the zone depletion at the p–n junction in operating electronic devices during its degradation [13]. The energy of captured electrons are released as high localized phonons giving rise to a phonon quick which increases the local temperature and causing the ddamage of p–n junction. The phonon–quick is followed by a coherent capture of a hole which by interaction with the electrons forms are very instable exciton [14].

In chalcogenid glasses it was observed a killing effect due to Fe^{2+} [15]. The non–radiative process was assumed, with the electron–hole recombination forming first an exciton which couples highly with the lattice phonons, decaying in such a way which is consistent with the phonon–quick.

The subject of the present report is the study of the killing effect of Fe^{3+} in barium aluminoborate glass, complementing the study of similar effect of Fe^{2+} in chalcogenide glass, and so obtain a complete view of the killing effect of Fe in amorphous materials.

II. EXPERIMENTAL PROCEDURES

The barium aluminoborate glasses were obtained by melting a mixture of $Ba(OH)_2$, H_3BO_3 and Al_2O_3 in platinum crucibles at 1300°C for 2h. The samples were annealed at 500°C for 24h. For this work we chose samples of $30BaO \cdot 50B_2O_3 \cdot 20Al_2O_3$ (at %). Different concentrations of Fe were obtained by addition of Fe_2O_3 and Fe_2SO_4. The sample E_4 was furnished by A. Bishay; made in American University, Cairo, Egypt; in alumina crucibles at 1340°C for 2½h; with $30BaO \cdot 60B_2O_3 \cdot 10Al_2O_3$ (at %). The sample A_{2T} was obtained by annealing the sample A_2 in a reducing acethylen flame for 4h. The sample A'_{2T} was obtained by exposure the sample A_{2T}, after a TL measurement, to $400 - \omega$ mercury lamp (unfiltered) for 1h at liquid nitrogen temperature. Samples for EPR (2 by 2 by 6mm) and TL (5 by 10 by 1.5mm) were cut.

The EPR measurements were done using a X–band Bruker spectrometer at room temperature.

The TL measurements were done using an apparatus assembled in our laboratory. The temperature was controlled with a home made cryostat in which a cold finger at IMPA (10^{-5} torr) was heated through an electrical resistor. The temperature was measured with

a Chrommel–Alumel thermocouple. The TL light was obseerved through a glass window, and detected with a Hamamatsu R910 photomultiplier and amplified with a home made electrometer (OP Intersil ICH 8500/ACTV). The samples were X irradiated at 77K (M_0; 40 kV; 20 mA) through an aluminium thin sheet window.

The optical absorption measurements were done using a Carl–Zeiss DMR 21 spectrophotometer.

III. EPR RESULTS

A typical EPR spectrum of $30BaO{\cdot}60B_2O_3{\cdot}10Al_2O_3$ glass (B_2) is shown in figure 1. The characteristic EPR lines [16,17] of Fe^{3+} in the glass network, are easily

Insert Figure 1

identified. The resonance at $g = 4.3$ is associated to the rhombic distortions of the crystal field at a tetrahedral or octahedral site [18] with $E/D \sim 1/3$. The Kramers shift arises a strong line at $g = 4.3$ independent of the axial direction and several lines depending on the axial direction. In glass the sum over all directions cancel all the axial dependent lines resulting in a single line at $g = 4.3$. The D values are estimated using the Aasa [19] diagram, given values around 1.5 and 3 cm^{-1}. The small resonance at $g = 2$ is associated to Fe^{3+} at substitutional octahedral site [20]. The small resonance at $g = 10$ is associated to interstitial Fe^{3+} ions [16].

Concentrations of Fe^{3+} with $g = 4.3$ were determined from EPR spectra calculating the area under the absorption curve, normalized by mass and the measuring amplification. For standard it was used samples B_1 and B_2, the biggest Fe doped

samples. The relation between the areas of $g = 4.3$ lines of samples B_1 and B_2 gives 1.6 as expected from the doping concentrations of Fe. The error in the integration of the EPR signal as well as the loss of Fe EPR signal due to the convertion of 5% of doped sample in Fe^{2+} was estimated to be about 7%. Then error of about 7% was assumed to all determinations of Fe^{3+} concentrations.

The concentrations of Fe^{3+} as compared to doping are given in table I. In low

Insert Table 1

doped samples, bigger concentrations of Fe^{3+} were found, due to Fe impurities in the materials used in the preparation of glasses.

Small concentrations of Fe^{2+} in the present glasses was shown by optical absorption spectroscopy. Only samples A_1, B_1 and B_2, the biggest doped samples showed a large and asymmetric absorption around 9500 cm^{-1} (figure 2). This is an indication

Insert Figure 2

that Fe^{2+} are subject to a distribution of magnitudes of axial fields.

Samples D_2 and G_2 were doped with the same at % concentration of Fe. However, the measured concentration of Fe^{3+} is smallest in G_2 sample. Thus, the Fe_2SO_4 doped G_2 glass has bigger Fe^{2+} concentration than D_2 sample. This is because Fe_2SO_4 doped the glass with Fe^{2+} ions, and the time at which the glass was mantained at 1300°C (2h) was not enough to reach ferric–ferrous equilibrium (at 5% Fe^{2+}). The equilibrium ferric–ferrous is expected to reach at longer times, as in silicate glasses it was found to be 20h at 1400°C [21].

IV. TL RESULTS

TL emission at temperatures between 77K and room temperature were observed in samples A_2, A_3, D_2, D_3, E_0, E_4, F_2 and G_2. Samples A_1, B_1 and B_2 does not show measurable TL emission. An example of TL curve is shown in figure 3.

Insert Figure 3

Activation energy of the TL process were determined for the samples E_0 and E_4 using the method of initial rise [22]. The correlation between the ln of the TL intensity and $1/T$ used in the initial rise is shown in figure 4. The activation enerrgy was

Insert Figure 4

determined accordingly with the approximation:

$$\ln I = -\Delta E/kT + \ln(sn^b)$$

where it was assumed a b–th order kinetic process, s is the frequency factor and n is the population of carriers. The values of ΔE are (0.21 ± 0.05)eV for E_0 and (0.22 ± 0.05)eV for E_4.

The chemical composition of the sample E_0 and E_4 are different. However, the activation energy obtained for these samples are almost the same. Then we conclude that the activation eneergy is not changed by changing the chemical composition of the samples by about 10 at %.

The TL curves area are shown in table 2. The TL area decreases as

Insert Table 2

Fe^{3+} concentration increases, as shown in figure 5. The correlation show that the TL area

Insert Figure 5

has roughly an inverse exponential dependence on the Fe^{3+} concentration.

The TL intensity of E_4 is about 1/3 of the sample E_0 with similar concentration of Fe^{3+}. As E_4 was prepared from available materials without doping at 1340°C for $2\frac{1}{2}$h, the concentration of Fe^{2+} is probably the same of E_0. Then, the difference between the intensities of E_0 and E_4 must be assigned to the differences in the glass composition, which changed from $30BaO \cdot 60B_2O_3 \cdot 10Al_2O_3$ to $30BaO \cdot 50B_2O_3 \cdot 20Al_2O_3$ (at %).

The samples D_2 and G_2 were prepared with the same at % concentration of Fe, but the former were doped with Fe^{3+} ions (Fe_2O_3) and the latter with Fe^{2+} ions (Fe_2SO_4). Thus concentration of Fe^{3+} in D_2 could be bigger than in G_2. The TL area of D_2 is different from TL area of G_2 within the limit of the experimental error. This is explained if we assume that Fe^{2+} also kill the TL emission.

The concentration of Fe^{3+} in D_2 is 6.1×10^{18} atoms/cm^3. Assuming that 5 at % of Fe is in Fe^{2+} state, there is 0.3×10^{18} atoms/cm^3 of Fe^{2+}, and 6.4×10^{18} atoms/cm^3 of iron. The same at % of Fe atoms were added in the preparation of D_2 and G_2. Also, the materials with which the samples were prepared are from the sames sources (bottles). Then, probably, there is 6.4×10^{18} atoms/cm^3 of iron in G_2. As 4.3×10^{18} atoms/cm^3 of Fe^{3+} was found in G_2, there is 2.1×10^{18} atoms/cm^3 of Fe^{2+}. Assuming that the dependence of TL area on the concentrations of Fe^{3+} and Fe^{3+} is exponential, and assuming 5 at % of Fe^{2+} in all samples but G_2, we fit an expression:

$$A = 55 \times 10^{10}\, A_{min} \exp\left\{-0.32N(Fe^{3+}) - 0.58N(Fe^{2+})\right\} \qquad (2)$$

where $N(Fe^{3+})$ and $N(Fe^{2+})$ are the concentrations of Fe^{3+} and Fe^{2+}, respectively, and A is the area under the TL curve. The calculated values of TL area using equation (2) are shown in table 2.

V. DISCUSSSIONS

If Fe^{3+} ions occupy the interstitial positions in the glass network, the EPR spectra cannot show the sharp and well defined lines at $g = 4.3$ [16]. If a tetrahedral unit has a non–bridging oxygen it attracts a second positive ion. In the present glasses, the interstitials are occupied by Ba^{2+} ions. The Ba^{2+} single ion around a non–bridging oxygen has not symmetry to produce a $g = 4.3$ line. But if two of these tetrahedrals joined each other, with two Ba^{2+} ions attracted by the two non–bridging oxygens situated at the opposite edges of the double tetrahedron it results in a symmetry compatible with $g = 4.3$. The structure of double tetrahedron B_2O_7 is the structure of lower energy of formation [23]. Thus the most probable structure for Fe^{3+} ion site is at double tetrahedron substituting B. In barium aluminoborate glasses it is supposed that almost all Al^{3+} ions occupy substitutional sites. In figure 6 we show a sketch of the site of Fe^{3+}.

Insert Figure 6

In tetrahedral site, there is a strong interaction of the external orbitals of Fe^{3+} with the p–orbital of the neighbour oxygens forming molecular orbitals [24]. This promotes a considerable delocalization of the exterrnal orbitals of Fe^{3+} [25].

The TL emission is killed by doping with Fe^{3+} at concentrations bigger than 0.1 at %. Assuming an uniform distribution of Fe for 0.1 at % and that the principal source of TL killing is Fe^{3+}, we calculate the volume of killing as being $V_{Fe} = 6.7 \times 10^{-2}\ cm^3$. Considering a spherical volume it corresponds to a radius of about 25Å.

The fraction of tetracoordinated B atoms for the present molar fraction of BaO is calculated to be 0.36 using the formula at the reference 25. Multiplying this value with V_{Fe} and we obtain the number of tetrahedrals localized around the radius of action of Fe^{3+} as being 460 tetrahedrals.

The above observations suggests that the antibonding orbitals have energy closer to the conduction band and the mixing of the Fe^{3+} antibonding orbitals and the extended oxygen p orbitals of oxygen extend the Fe^{3+} antibonding orbitals over the 460 tetrahedrals and radius 25Å.

It was suggested [14] that the non–radioactive recombination at deep levels introduced by defects or impurities in semiconductors occur through the multiphonon emission at the neighbour of the defect. In this model the multiphonon emission is promoted after the capture of an electron or hole. The huge localized vibrations, stimulated a coherent capture of a carrier of opposite signal of the first one, resulting in a non–radioactive electron–hole recombination with a new huge emission of phonons. The efficiency, Y, of capture of a majority carrier after a capture of a minority carrier is given by:

$$Y = 1 - \exp\left[-\nu(n_2/n_{2T})(2\pi f_2/\omega)\right] \ , \qquad (3)$$

where ν is the number of times that the systems acquire an energetic configuration good for capture; n_2 is the density of free majority carriers; n_{2T} is the effective density of states for free majority carriers; f_2 is the scape frequency by the majority carrrieer and $\omega/2\pi$ is the lattice vibrational frequency.

In the present case, n_2 is the density of sites under the action of Fe, $n_2 = N(Fe^{3+}) + N(Fe^{2+})$, if for each non–radioactive recombination there is a hole (BOHC) within the range of action of Fe. Being Y the efficiency of non–radioactive capture of an electron, the luminescence efficiency, Z, is the complementar factor. Then, considering two killing species, Fe^{2+} and Fe^{3+}, we obtain

$$Z = 1/\exp\{a\,N(Fe^{2+}) + b\,(Fe^{2+})\} \quad , \tag{4}$$

where a and b are the factor $(N/n_{2T})(2\pi f_2/\omega)$ for Fe^{2+} and Fe^{3+}. Then, $A = A_0 Z$, where A_0 is the luminescence without quenching. As $a = 0.58 \times 10^{-18}\ cm^3$ and $b = 0.32 \times 10^{-18}\ cm^3$, with $A_0 = 54$, the quenching effect is bigger for Fe^{2+}.

In figure 7, we show a sketch of the processes of non–radioactiove electron–hole

Insert Figure 7

recombination, through extended antibonding orbitals of Fe. The relaxation of captured electron through multiphonon emission release hole from BOHC, which is attracted by this electron forming a very short lifetime exciton. This exciton is annihilated through another multiphonon emission.

In figure 8, we show a sketch of the glass network with Fe^{3+} ion site and an

Insert Figure 8

electron–hole recombination through multiphonon process.

The TL emission of E_4 is about 1/4 of E_0, although the Fe concentration is almost the same magnitude. The former sample have the chemical composition

$30BaO \cdot 60B_2O_3 \cdot 10Al_2O_3$ and the latter $30BaO \cdot 50B_2O_3 \cdot 20Al_2O_3$. It was shown [26] that the increasing concentrations of BaO and/or Al_2O_3 increases the concentration of tetracoordinated Fe^{3+}. Thus increasing the amount of Al_2O_3, produces bigger amounts of double coordinated B_2O_7 units, and as consequence larger amounts of precursor defects of BEC and BOHC. Therefore, irradiation produces larger concentrations of trapped carriers in E_0, which is consistent with the observation of bigger luminescence in E_0.

CONCLUSIONS

In the present work we studied the quenching of the thermoluminescence by Fe ions in aluminoborate glass. The quenching is total, in the limit of the observation of our equipment, from concentrations above 0.1 at % of Fe.

The activation energy was shown to be about $\Delta E = 0.21$ ev for samples with 10 at % of difference in B_2O_3 and Al_2O_3, meaning that the activation energy is not sensitive to small changes in the concentrations of these components. This effect suggests that the electron traps are far apart, enough to prevent interaction between them.

Otherwise, the TL intensity is bigger for the sample with bigger Al_2O_3 concentration. This effet is probably the consequence of the increasing of double coordinated B_2O_3 units in samples of bigger amounts of Al_2O_3. The B_2O_3 units are the source of precursor centers of BEF and BOHC.

The TL efficiency was observed to decrease exponentially with increasing concentration of Fe. Assuming that the quenching is due to the coherent capture of holes due to the multiphonon emission after the capture of an electron at Fe^{3+} or Fe^{2+} ions, we were able to fit the TL intensity using the Sumi's exponential expression. Then the fitted parameters show that the quenching effect of Fe^{2+} ion is bigger than of Fe^{3+} ion.

REFERENCES

1. W.M. Pontuschka, S. Isotani and A. Piccini, "Optical and Thermal Bleaching of X–Irradiated Barium Aluminoborate Glasses", J. Am. Ceram. Soc., 70, 59–64.
2. T.K. Bansal and R.G. Mendiratta, J. Non–Crystalline Solids, 86, 13–21 (1986).
3. N.G. Leite, "*Thermoluminescence of E'centers in Barium Aluminoborate Glasses*", Master Dissertation, IFUSP (1988).
4. S.M. Del Nery, "*Luminescence in Barium Aluminoborate Glasses in the Presence of Quenching Processes*", Doctoral Thesis, IFUSP (1990).
5. M. Schön, Z. Phys., 119, 470 (1942).
6. H.A. Klasens, Nature, 158, 306 (1946).
7. F. Urbach, A. Urbach and M. Schwartz, J. Opt. Soc. Am., 37, 122 (1947).
8. H.A. Klasens, W. Ramsden and C. Quantie, J. Opt. Soc. Am., 38, 60 (1947).
9. N.R. Nail, F. Urbach and D. Pearlman, J. Opt. Soc. Am., 39, 690 (1949).
10. R.H. Bube, S. Larach and R.E. Shader, Phys. Rev., 92, 1135 (1953).
11. C.A. Duboc, Brit. J. Appl. Phys. Suppl. 4, 107 (1955).
12. H.A. Klasens, J. Phys. Chem. Solids, 7, 175 (1958).
13. Gold and Weisberg,
14. H. Sumi, J. Lum., 40 & 41, 76 (1988).
15. S.G. Bishop and P.C. Taylor, Phil. Mag., B40(6), 483 (1979).
16. T. Castner Jr., G.S. Newell, W.C. Holton and C.P. Slichter, J. Chem. Phys., 32, 668–673 (1960).
17. D.L. Griscom, "Borate Glass Structure", edited by L.D. Pye, V.D. Frechette and N.J. Kreidl (Plenum, 1978) p. 115–128.
18. D.W. Moon, J.M. Aitken, R.K. MacCrone and G.S. Cieloszyk, Phys. Chem. Glasses, 16, 91 (1975).

19. R. Aasa, J. Chem. Phys. 52, 3919 (1970).

20. A.R. Blak, S. Isotani and S. Watanabe, Phys. Chem. Minerals, 8, 161–166 (1982).

21. C.G. Rouse and J. Willianson, Six Symposium on Special Ceramics Proceedings of Stoke–on–Trent, 91–125 (1974).

22. R. Chen, J. Mat. Science, 11, 1521–1541 (1976).

23. P. Beekenkamp, Philips Research Reports Suppl., 4 (1966).

24. C.J. Balhausen, "Introduction to Ligand Field Theory", Ed. McGraw–Hill (1962).

25. L.E. Orgel,

26. B.O. Mysen, D. Visgo, E.R. Neumann and F.A. Seifert, 70, 317 (1985).

Table 1. Area of EPR lines at $g = 4.3$ and concentrations of Fe^{3+}.

Sample*	Doping Fe (at %)	Area	N (10^8 spins/cm^3)
E_0	–	0.44 ± 0.03	1.13 ± 0.08
A_3	1×10^{-3}	0.77 ± 0.05	2.1 ± 0.2
D_3	2×10^{-3}	0.80 ± 0.06	2.9 ± 0.2
A_2	1×10^{-2}	1.9 ± 0.1	4.8 ± 0.3
D_2	2×10^{-2}	2.4 ± 0.2	6.1 ± 0.6
F_2	4×10^{-2}	4.4 ± 0.3	11 ± 0.8
G_2	2×10^{-2}	1.7 ± 0.1	4.3 ± 0.3
A_1	0.1	5.9 ± 0.4	15 ± 1
B_1	0.5	38 ± 3	96 ± 9
B_2	0.8	61 ± 4	50 ± 10
E_4	–	0.45 ± 0.003	1.1 ± 0.08

*All samples were doped with Fe_2O_3, except sample G_2 which was doped with Fe_2SO_4.

Table 2. TL emission compared to Fe^{3+} concentration.

Sample	TL (10^{-10} A min)	A* (10^{-10} A min^2)	N(Fe^{3+}) (10^{18} spins/cm^3)	N(Fe^{2+})** (10^{18} spins/cm^3)
E_0	37.0 ± 0.5	36.3	1.13 ± 0.08	0.06
A_3	25.7 ± 0.5	25.9	2.1 ± 0.2	0.11
D_3	19.0 ± 0.5	19.5	2.9 ± 0.2	0.15
A_2	12.0 ± 0.5	10.1	4.8 ± 0.3	0.24
D_2	6.3 ± 0.5	6.4	6.1 ± 0.6	0.31
F_2	1.9 ± 0.5	1.1	11 ± 0.8	0.55
G_2	4.1 ± 0.5	4.1	4.3 ± 0.3	2.10

* Calculated from equation 2.

**Estimated values with $[Fe^{2+}] = 0.05\ [Fe]$; $[Fe] = [Fe^{2+}] + [Fe^{3+}]$.

FIGURE CAPTIONS

Figure 1. EPR spectrum of $30BaO \cdot 60B_2O_3 \cdot 10Al_2O_3$ (at %) glass B_2 at room temperature.

Figure 2. Optical absorption spectra of glass samples A_1, A_2, B_1 and B_2.

Figure 3. TL curve of glass sample A_3.

Figure 4. Natural logarithm of the initial raise TL intensity versus reciprocal of the absolute temperature of samples (a)E_0 and (b)E_4.

Figure 5. Relation between the TL intensity versus Fe^{3+} concentration.

Figure 6. Sketch of the Fe^{3+} ion site in glass network.

Figure 7. Sketch of non–radioactive electron–hole recombination.

Figure 8. Sketch of coherent electron–hole capture.

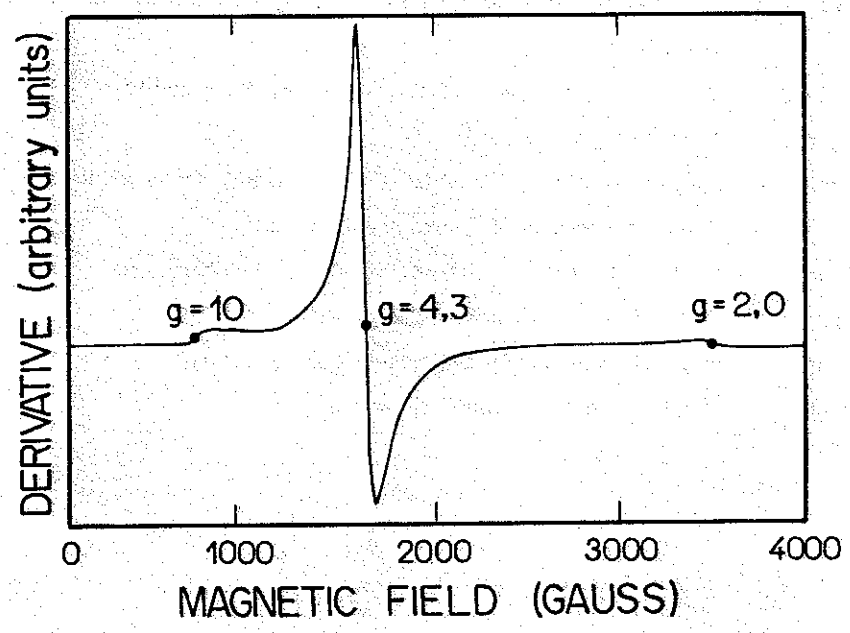

FIGURE 1

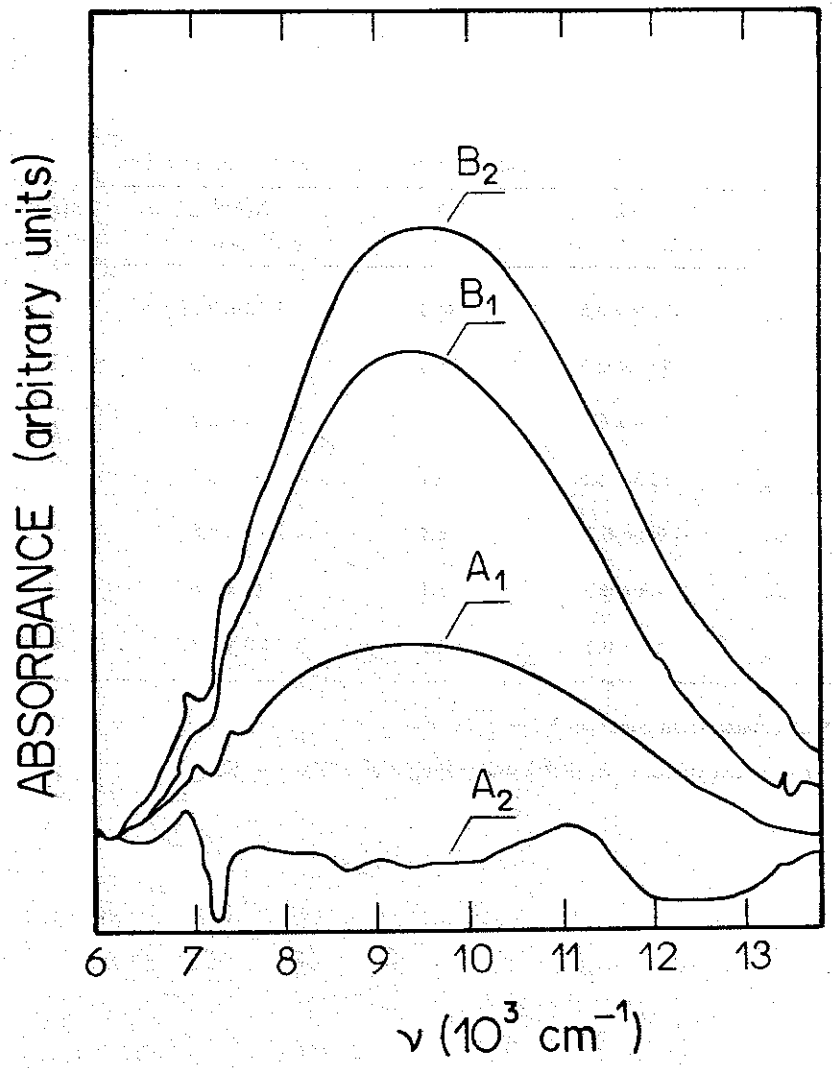

FIGURE 2

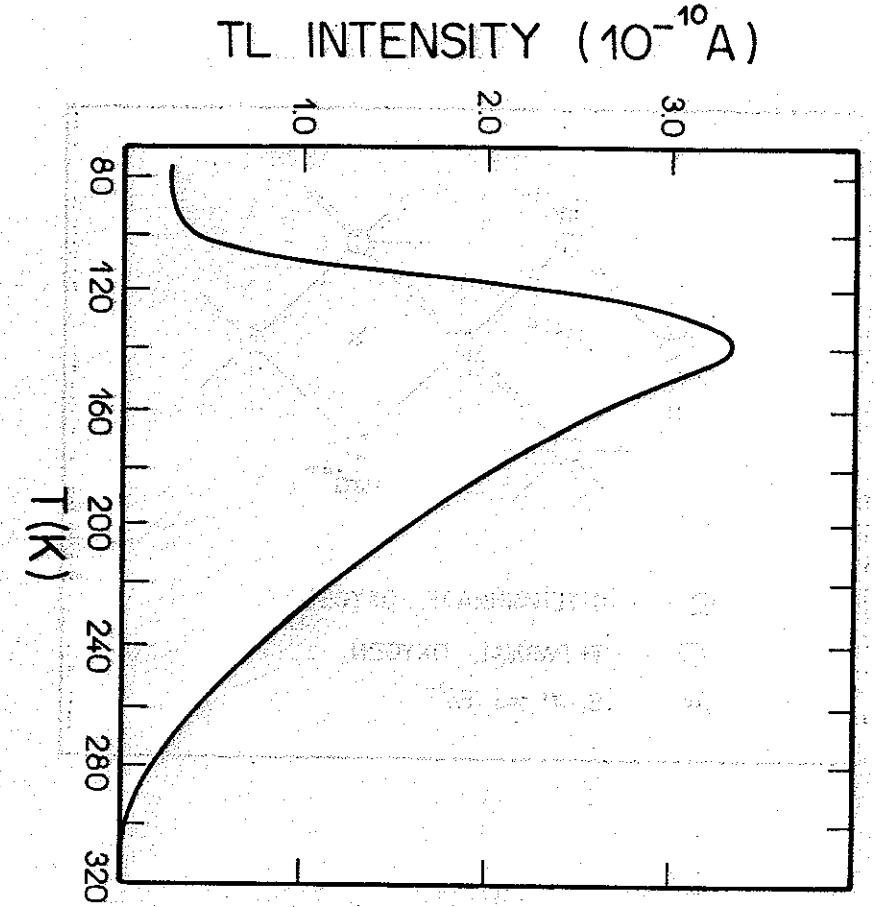

FIGURE 3

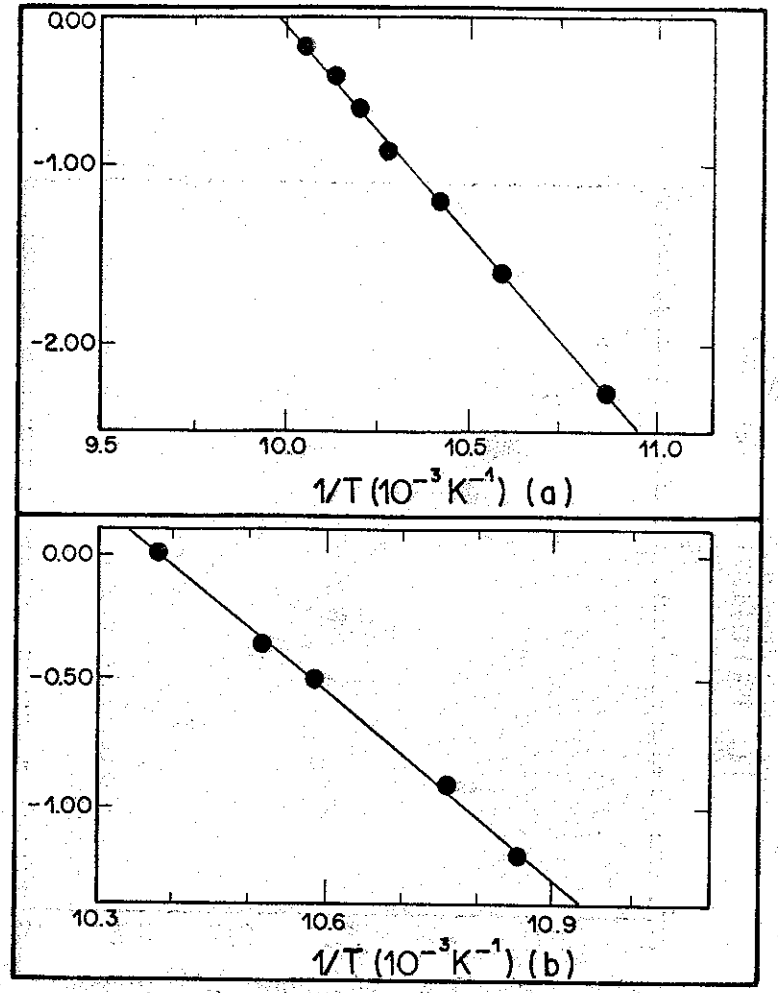

FIGURE 4

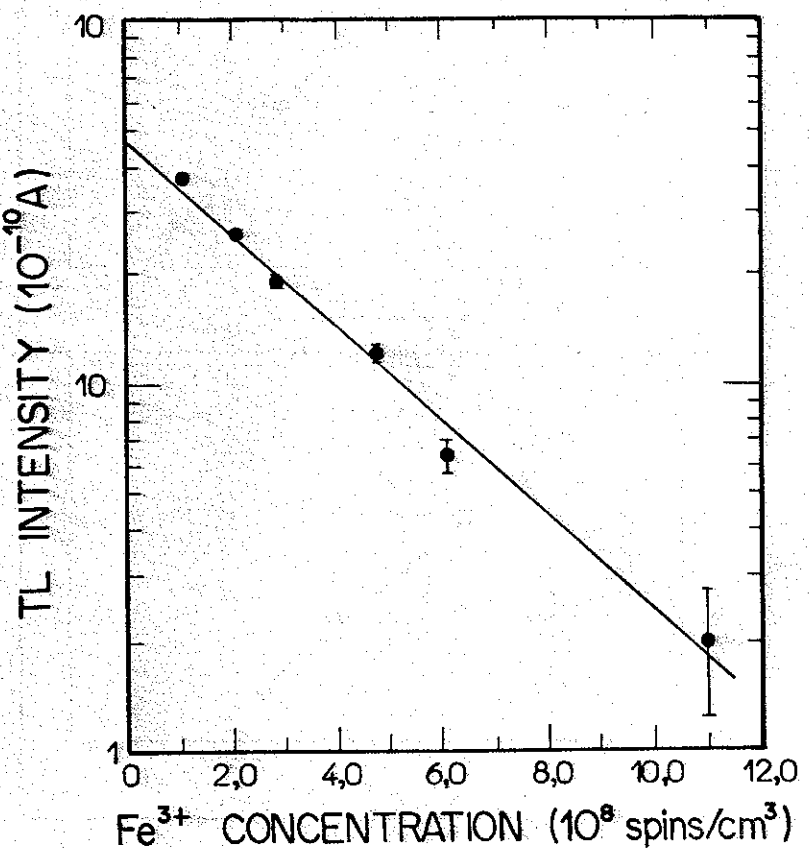

FIGURE 5

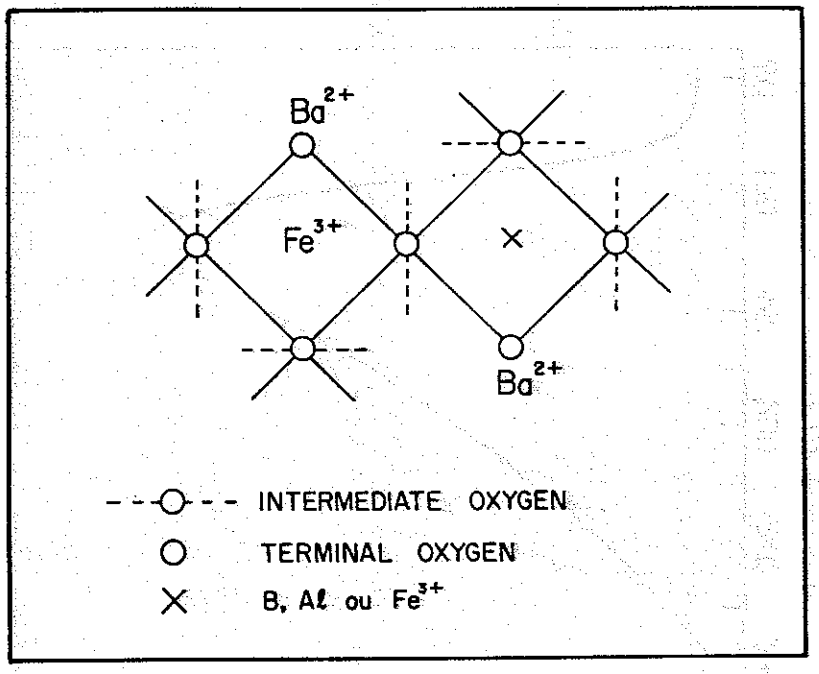

FIGURE 6

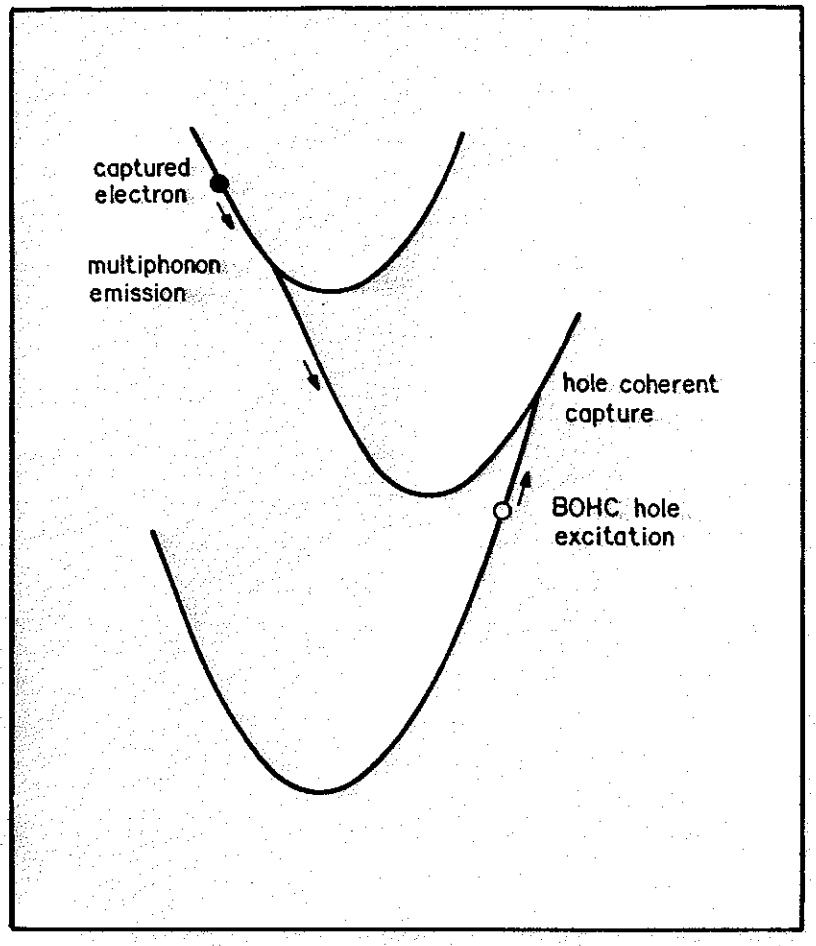

FIGURE 7

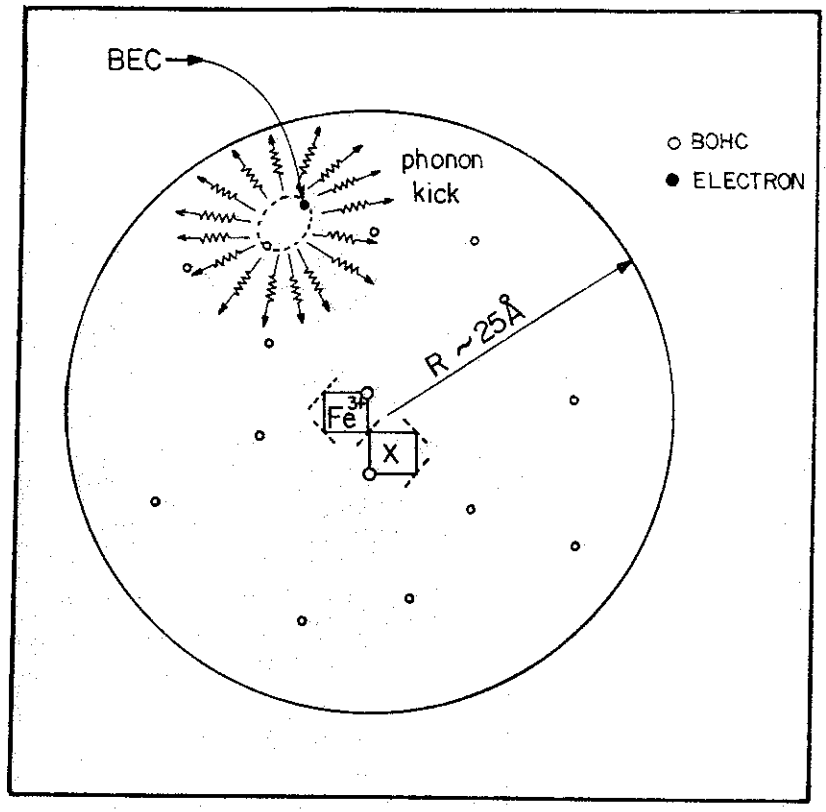

FIGURE 8